Journal of Experimental and Theoretical Physics, Vol. 101, No. 3, 2005, pp. 554–561.
Translated from Zhurnal Éksperimental'noĭ i Teoreticheskoĭ Fiziki, Vol. 128, No. 3, 2005, pp. 645–654.

ELECTRONIC PROPERTIES OF SOLIDS

Interface Phonons in Semiconductor Nanostructures with Quantum Dots

M. Yu. Ladanov[a], A. G. Milekhin[a, *], A. I. Toropov[a], A. K. Bakarov[a], A. K. Gutakovskii[a], D. A. Tanne[b], S. Schultze[c], and D. R. T. Zahn[c]

[a]*Institute of Semiconductor Physics, Siberian Division, Russian Academy of Sciences, pr. akademika Lavrent'eva 13, Novosibirsk, 630090 Russia*

**e-mail: milekhin@thermo.isp.nsc.ru*

[b]*Department of Physics, Pennsylvania State University, 104 Davey Lab., University Park, PA 16802, USA*

[c]*Institut für Physik, Technische Universität Chemnitz, D-09107, Chemnitz, Germany*

Received April 21, 2005

Abstract—The vibrational spectrum of structures with InAs quantum dots in an AlGaAs matrix and AlAs quantum dots in an InAs matrix is investigated experimentally and theoretically. The Raman scattering spectra of light exhibit features that correspond to transverse-optical (TO), longitudinal-optical (LP), and interface phonons. The frequencies of interface phonons in InAs and AlAs quantum dots in an AlGaAs matrix with various concentrations of aluminum are calculated with the use of experimental values of transverse- and longitudinal-optical phonons in the approximation of a dielectric continuum. It is shown that the model of a dielectric continuum adequately describes the behavior of interface phonons in structures with quantum dots under the assumption that the quantum dots are spheroidal. © *2005 Pleiades Publishing, Inc.*

1. INTRODUCTION

Periodic semiconductor structures with self-organized quantum dots, which are characterized by unique electronic and optical properties, are one of the most challenging objects of research in semiconductor physics. These objects attract interest in view of the possibility to design, on the basis of these objects, new devices, such as quantum transistors, high-speed memory elements, narrow-band light-emitting diodes, heterojunction lasers, and infrared (IR) photodetectors [1–3].

Progress in the epitaxial growth technology has allowed one to produce quantum-dot structures with controllable properties on the basis of a series of materials (InAs/Ga(Al)As, In(Ga)As/InP [4, 5], Ge/Si, GaSb/InP, GaN/AlN) [6–9]. The most thoroughly investigated system is InAs/Ga(Al)As; a large number of papers has been devoted to the study of its optical and electronic properties [2]. However, despite the fact that the vibrational spectrum contains information about the structural properties (the size, dispersion of size, and the shape) of quantum dots [10, 11] and mechanical stress in nanostructures [12, 13], the vibrational properties have been poorly studied even in this system. The most widespread methods for studying vibrational spectra are the Raman spectroscopy and the infrared (IR) spectroscopy. These methods are complementary because they use different selection rules; therefore, they allow one to study vibrational excitations of different types of symmetry. The Raman and IR spectroscopy have been applied to study optical phonons in stressed [13, 14] and relaxed [12, 15] quantum dots, in quantum dots of InGaAs solid solutions [16], and in a wetting layer [17, 18].

Earlier, a theoretical analysis of the spectrum of optical phonons in quantum dots was carried out within the model of valence-force fields [19, 20] and in the approximation of a dielectric continuum [15]. The model of valence-force fields is an empirical atomistic 1
model and allows one to calculate the phonon frequencies in quantum dots consisting of a few thousand atoms. Calculations with the use of this model involve large arrays of data; this makes these calculations rather tedious. The approximation of a dielectric continuum is a macroscopic model and can rather easily be applied to the calculation of the frequencies of interface phonons localized near the interface between the materials of the quantum dots and the matrix [21].

The simplest model of a dielectric continuum deals with spherical quantum dots of one material embedded into the matrix of another material [22, 23]. In this case, the eigenfrequencies are determined from the condition 2

$$\frac{\epsilon_1(\omega_{lm})}{\epsilon_2(\omega_{lm})} = -1 - \frac{1}{l} \qquad (1)$$

where ϵ_1 and ϵ_2 are the dielectric functions of the quantum dots and the matrix, respectively; ω_{lm} are the eigen- 2
frequencies of interface phonons; and l is a quantum number of a phonon ($l = 1, 2, \ldots$).

As a rule, the shape of a real quantum dot is different from a sphere [24, 25] (a truncated pyramid for a sys-

tem of InAs quantum dots in a GaAs matrix [26], a hemisphere for Ge quantum dots in a Si matrix [27], and an ellipsoid for AlAs quantum dots in an InAs matrix [28]). Therefore, the model of a dielectric continuum was further developed in [29] and [30], where it was assumed that quantum dots are spheroidal. The reduction of the symmetry of quantum dots from spherical to spheroidal complicates the condition for the 2 eigenfrequencies of interface phonons: these frequencies will now depend on two quantum numbers, l and m.

In [30], the dielectric function of a matrix is considered that does not depend on frequency; this provides a unique set of interface modes whose frequencies lie between the frequencies of transverse-optical (TO) and longitudinal-optical (LO) phonons in quantum dots. Such an approach is justified if a model deals with quantum dots in a vitreous or an organic matrix.

In [29], it was assumed that the dielectric functions of both the quantum dots and the material of the matrix depend on frequency; unlike the dielectric-continuum model [30], this yields two sets of interface modes. The first set, which refers to quantum dots, lies in the spectral range between TO and LO phonons in the material of quantum dots. The other set lies in the frequency range between the corresponding values of bulk phonons in the matrix material.

Despite the progress made in the theoretical description of interface phonons in spheroidal quantum dots, there is a lack of experimental study of interface phonons in structures with self-organized quantum dots [13, 11].

In this paper, we present the results of investigating interface phonons in structures with InAs and AlAs quantum dots by the methods of Raman spectroscopy and compare them with the data obtained by calculating the interface phonons in the approximation of a dielectric continuum.

2. THEORY

Let us write out the basic equations necessary for the analysis of the dielectric-continuum approximation in polar materials [30, 31]. The Born–Huang equation of motion can be represented as follows:

$$\ddot{w} = -\omega_{TO}^2 w + \sqrt{\frac{\epsilon_0 - \epsilon_\infty}{4\pi}\omega_{TO}^2}E, \qquad (2)$$

where the polarization P can be expressed as

$$P = \sqrt{\frac{\epsilon_0 - \epsilon_\infty}{4\pi}\omega_{TO}^2}w + \frac{\epsilon_\infty - 1}{4\pi}E. \qquad (3)$$

Here, $w = \sqrt{N\mu}\,u$ is a relative displacement between a pair of ions with reduced mass μ in a crystal with concentration N, E is the electric field, ω_{TO} and ω_{LO} are the frequencies of transverse- and longitudinal-optical phonons, and ϵ_0 (ϵ_∞) is the static (high-frequency) dielectric constant of a polar material. In addition, we assume that the Lidden–Sacks–Teller relation $\omega_{LO}^2/\omega_{TO}^2 = \epsilon_0/\epsilon_\infty$ holds.

For the electric field to satisfy the Maxwell equations, it is necessary that the electric displacement

$$\mathbf{D} = \epsilon(\omega)\mathbf{E} = \mathbf{E} + 4\pi\mathbf{P}$$

should satisfy the Hertz equation

$$\nabla \cdot \mathbf{D} = 0.$$

Using the relation

$$\mathbf{E} = -\nabla\varphi,$$

we can write out the basic equation of dielectric approximation:

$$\epsilon(\omega)\nabla^2\varphi = 0. \qquad (4)$$

It is assumed that the time dependence of all the quantities introduced above is harmonic: $f(t) \propto \exp(-i\omega t)$. In the absence of damping, the frequency-dependent dielectric function $\varepsilon(\omega)$ of a polar material is defined by

$$\epsilon(\omega) = \epsilon_\infty\frac{\omega_{LO}^2 - \omega^2}{\omega_{TO}^2 - \omega^2}. \qquad (5)$$

Interface phonons are directly related to the electric potential, which must satisfy the Laplace equation $\nabla^2\varphi = 0$. Therefore, one of possible solutions to Eq. (4) is $\epsilon(\omega) \neq 0$ for $\omega \neq \omega_{LO}$. The boundary condition at the interface S between two media, the continuity of the normal components of D, is expressed as

$$\epsilon_1\left[\frac{\partial\varphi_1}{\partial n}\right]_S = \epsilon_2\left[\frac{\partial\varphi_1}{\partial n}\right]_S. \qquad (6)$$

Since the object of our study are interface phonons in spheroidal quantum dots, it is convenient to pass from Cartesian coordinates to spheroidal (prolate and 3 oblate) coordinate systems [30].

The prolate system of coordinates ξ, η, ϕ is used for 3 calculating the frequencies of interface phonons for oblate quantum dots and is expressed in terms of Cartesian coordinates as follows:

$$x = b\sqrt{(\xi^2 - 1)(1 - \eta^2)}\cos\phi,$$
$$y = b\sqrt{(\zeta^2 - 1)(1 - \eta^2)}\sin\phi, \qquad (7)$$
$$z = b\xi\eta,$$

whereas the oblate system of coordinates is convenient for determining the frequencies of interface phonons in prolate quantum dots: 3

$$x = b\sqrt{(\xi^2 + 1)(1 - \eta^2)}\cos\phi,$$

$$y = b\sqrt{(\xi^2+1)(1-\eta^2)}\sin\phi, \qquad (8)$$
$$z = b\xi\eta,$$

where $\xi \geq 1$ for the prolate system, $\xi \geq 0$ for the oblate system, and $-1 \leq \eta \leq 1$ and $0 \leq \phi \leq 2\pi$ for both systems. The expression ξ = const describes an ellipsoid of rotation with the rotation axis (z axis) directed along the principal axes of the ellipsoid; $2b$ is the interfocal distance.

Consider an elliptic surface defined by the formula $\xi = \xi_0$ = const. In our model, the interior domain defined by $1 \leq \xi \leq \xi_0$ for prolate and oblate systems of coordinates is one of polar semiconductors with the dielectric function $\epsilon(\omega)$ given by (5), where ω is an eigenfrequency corresponding to interface vibrations of a spheroidal quantum dot. The exterior, with respect to the elliptic surface, domain defined by the relation $\xi \geq \xi_0$ is an infinite medium with the dielectric function given by (5).

The Laplace equation can be separated in prolate spheroidal coordinates; a solution to the above-described model can be sought for in the form

$$\varphi^< = A_{lm}R_l^m(\xi)Y_{lm}(\eta,\phi), \quad \xi \leq \xi_0,$$
$$\varphi^< = A_{lm}\frac{R_l^m(\xi_0)}{Q_l^m(\xi_0)}Q_l^m(\xi)Y_{lm}(\eta,\phi), \quad \xi \geq \xi_0, \qquad (9)$$

where A_{lm} are Fourier coefficients and $Y_{lm}(\eta, \phi)$ are ordinary harmonic spherical functions. The same expression applies to the oblate system of coordinates after certain transformations and the replacement $\xi \longrightarrow i\xi$.

The functions $R_l^m(\xi)$ and $Q_l^m(\xi)$ in Eq. (9) are expressed in terms of hypergeometric functions $F[x]$:

$$R_l^m(\xi) = \frac{(2l)!(\xi^2-1)^{m/2}\xi^{l-m}}{2^l l!(l-m)!}$$
$$\times F\left[\frac{m-l}{2}, \frac{m-l+1}{2}, \frac{1}{2}-l, \frac{1}{\xi^2}\right],$$
$$Q_l^m(\xi) = \frac{2^m(l-m)!\Gamma(1/2)(\xi^2-1)^{m/2}}{\Gamma(l+3/2)(2\xi)^{l+m+1}} \qquad (10)$$
$$\times F\left[\frac{l+m+1}{2}, \frac{l+m+2}{2}, l+\frac{3}{2}, \frac{1}{\xi^2}\right],$$

where $\Gamma(x)$ is the gamma function. For the oblate system of coordinates, these functions are expressed in similar terms; however, after the replacement $\xi \longrightarrow i\xi$ and certain algebraic transformations, they can be represented as the following functions of $i\xi$:

$$R_l^m(i\xi) = \frac{(2l)!(\xi^2-1)^{m/2}\xi^{l-m}}{2^l l!(l-m)!}$$
$$\times F\left[\frac{m-l}{2}, \frac{m-l+1}{2}, \frac{1}{2}-l, -\frac{1}{\xi^2}\right],$$
$$Q_l^m(i\xi) = \frac{2^l l!(l-m)!(\xi^2-1)^{m/2}\xi^{-l-m-1}}{(2l+1)!} \qquad (11)$$
$$\times F\left[\frac{l+m+1}{2}, \frac{l+m+2}{2}, l+\frac{3}{2}, -\frac{1}{\xi^2}\right].$$

Here, the angular moments take the values $l = 1, 2, 3, \ldots$ and $|m| \leq l$.

For $\xi = \xi_0$, the boundary condition (6) defines the relations

$$f_{lm}^P(\xi_0) = \frac{\epsilon(\omega)}{\epsilon_D} \equiv \left(\frac{d}{d\xi}\ln Q_l^m(\xi)\Big|_{\xi_0}\right)\left(\frac{d}{d\xi}\ln R_l^m(\xi)\Big|_{\xi_0}\right)^{-1},$$
$$f_{lm}^O(\xi_0) = \frac{\epsilon(\omega)}{\epsilon_D} \equiv \left(\frac{d}{d\xi}\ln Q_l^m(i\xi)\Big|_{\xi_0}\right) \qquad (12)$$
$$\times\left(\frac{d}{d\xi}\ln R_l^m(i\xi)\Big|_{\xi_0}\right)^{-1}$$

for the prolate and oblate coordinate systems, respectively. The universal parameters f_{lm}^P and f_{lm}^O do not depend on the nature of the material and on the normalization of the functions R_l^m and Q_l^m; however, what is especially important, they depend on the geometry of quantum dots. The conditions

$$\frac{\omega_{lm}^2}{\omega_{\mathrm{TO}}^2} = \frac{\epsilon_0 - \epsilon_D f_{lm}^P(\xi_0)}{\epsilon_\infty - \epsilon_D f_{lm}^P(\xi_0)},$$
$$\frac{\omega_{lm}^2}{\omega_{\mathrm{TO}}^2} = \frac{\epsilon_0 - \epsilon_D f_{lm}^O(\xi_0)}{\epsilon_\infty - \epsilon_D f_{lm}^O(\xi_0)}, \qquad (13)$$

for the eigenfrequencies of interface phonons in prolate and oblate coordinate systems, respectively, allow one to calculate the frequencies of interface phonons.

Note that, in contrast to the case of spherical quantum dots, the eigenfrequencies of interface phonons depend on two quantum numbers, l and m, and on the parameter ξ_0. It can be shown that, for $\xi_0 \longrightarrow 0$, Eq. (13) yields the following relation for the eigenfrequencies in spherical quantum dots [31]:

$$\frac{\omega_l^2}{\omega_{\mathrm{TO}}^2} = \frac{\epsilon_0 l + \epsilon_D(l+1)}{\epsilon_\infty l + \epsilon_D(l+1)}, \qquad (14)$$

which is identical to formula (1).

For InAs quantum dots in the form of oblate spheroids in an AlAs matrix, the frequencies of interface modes as a function of the quantum number m for the semiaxis ratio $R_p/R_e = 1/2$ are shown in Fig. 1a. The semiaxis R_p lies in the plane of the layers of the structure, while R_e is perpendicular to the surface. Figure 1a

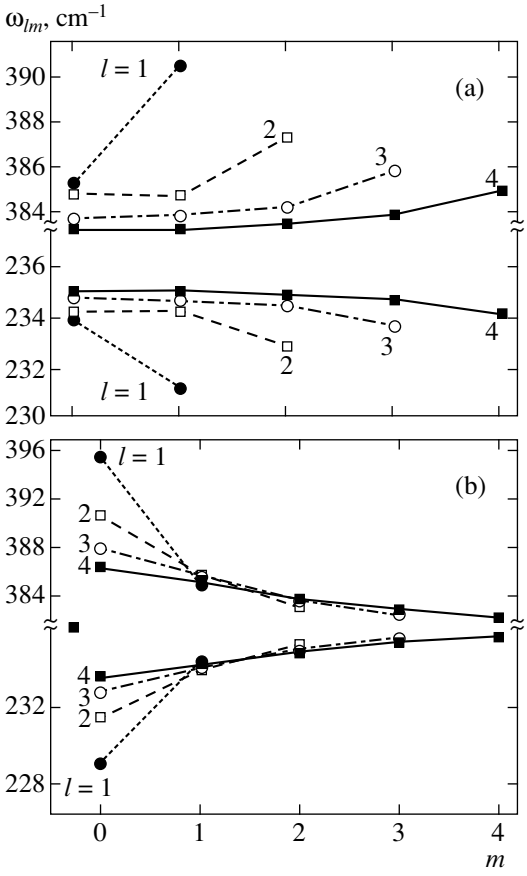

Fig. 1. Frequencies of interface modes in (a) oblate quantum dots for $R_p/R_e = 1/2$ and (b) prolate quantum dots for $R_p/R_e = 2$ as a function of the quantum numbers m and l. The frequencies of phonons with equal quantum numbers l and different numbers m are connected by lines.

shows that the calculated values of the frequencies of interface phonons in InAs quantum dots and in the AlAs matrix range within the limits of 230–236 cm^{-1} and 382–392 cm^{-1}, respectively, and lie between the frequencies of TO and LO phonons. As the quantum numbers of the calculated modes increase, the frequencies of these modes tend to the frequencies of interface phonons that propagate along plane heterojunction boundaries. For AlAs-like phonons, this value is equal to 383 cm^{-1}, whereas, for InAs-like phonons, it is equal to 235 cm^{-1}. Note that these values differ by several inverse centimeters from the frequencies of modes with small l and large m.

The set of frequencies of interface phonons for prolate quantum dots significantly differs form the relevant set for oblate quantum dots (Fig. 1b). This difference is especially significant for the frequencies of modes with small quantum numbers l and m.

In the model considered, the parameter that defines the shape of a quantum dot is the ratio R_e/R_p of large and small semiaxes.

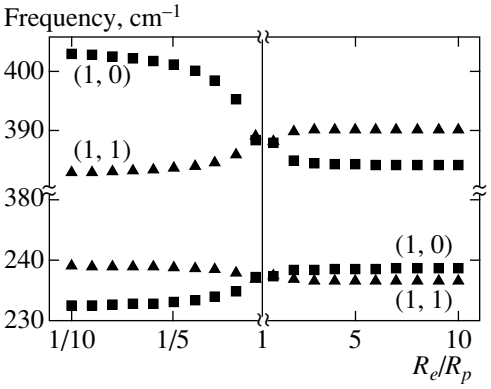

Fig. 2. Frequencies of interface phonons with quantum numbers (1, 0) and (1, 1) as a function of the ratio R_e/R_p for oblate (R_e/R_p = 1–10) and prolate (R_e/R_p = 1/10–1) quantum dots.

Figure 2 shows the frequencies of interface phonons in quantum dots with the quantum numbers (1, 0) and (1, 1) as a function of the ratio R_e/R_p. It is especially important to determine the frequencies of these modes, because it is the phonons with small quantum numbers (l, m) equal to (1, 0) and (1, 1) that should make the main contribution to the Raman scattering of light [29].

For the ratio R_e/R_p ranging from 1/10 to 1 (prolate quantum dots), the frequencies of the first modes of interface phonons are shown in the left-hand part of the diagram, whereas the appropriate frequencies for R_e/R_p ranging from 1 to 10 are shown in the right-hand part. One can see that the frequencies of interface phonons exhibit the greatest variation in those quantum dots whose shape is close to a sphere.

Consider the case when the material of either the matrix or the quantum dots is a ternary solution $A_xB_{1-x}C$. This case is of definite interest because structures with InGaAs/AlGaAs quantum dots are already available. Since the dielectric function of a solid solution (in the absence of damping) is given by

$$\epsilon_a(\omega) = \epsilon_\infty^a \frac{(\omega_{LO,1}^2 - \omega^2)(\omega_{LO,2}^2 - \omega^2)}{(\omega_{TO,1}^2 - \omega^2)(\omega_{TO,2}^2 - \omega^2)}, \qquad (15)$$

where $\epsilon_\infty^a = \epsilon_{\infty,1}x + \epsilon_{\infty,2}(1-x)$, the solution to Eq. (13) represents three sets of interface phonons one of which corresponds to the material of a binary compound and the two other sets correspond to the material of a solid solution. For example, for InAs/AlGaAs quantum dots, these sets represent interface phonons in InAs quantum dots and AlAs- and GaAs-like interface phonons in the matrix. Note that, for structures in which both the matrix material and the quantum dots represent solid solutions, one may expect that there exist four sets of interface phonons.

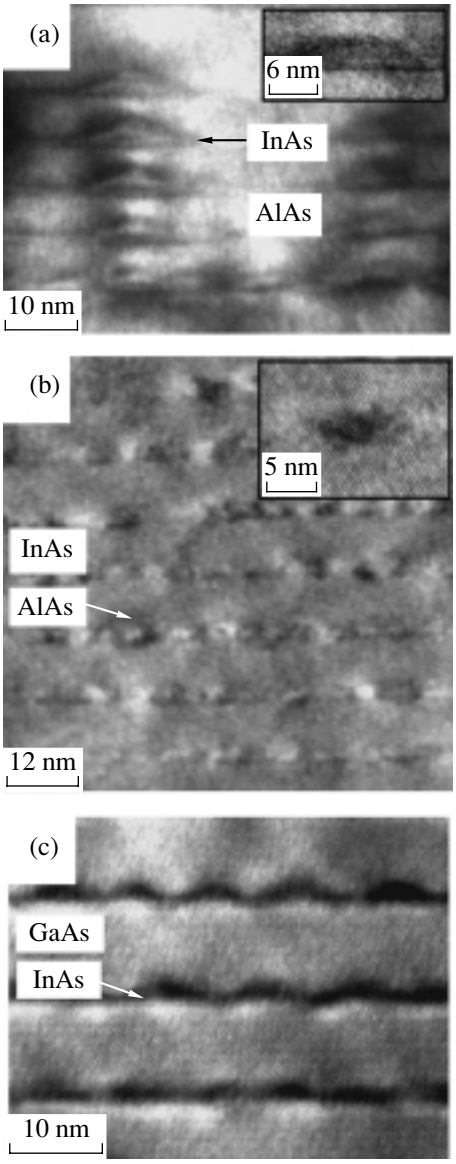

Fig. 3. Cross-sectional electron-microscope pictures of structures with InAs quantum dots in AlAs and GaAs matrices (samples A (a) and C (b), respectively) and AlAs quantum dots in an InAs matrix (sample B (b)). The insets represent detailed views of the quantum dots obtained at high resolution.

3. EXPERIMENTAL

The structures to be studied were grown on GaAs substrates in the Stranski–Krastanov growth mode by molecular beam epitaxy technique on a Riber 32P equipment. Sample A consisted of ten periods each of which contained a layer with InAs quantum dots of nominal thickness of 2.25 monolayers and an AlAs layer of thickness 25 nm. Sample B, consisting of 50 periods of AlAs quantum dots embedded into an InAs matrix, was grown on a silicon-doped ($N_{Si} = 2 \times 10^{18}$ cm^{-3}) InAs buffer layer of thickness 1.5 μm at a substrate temperature of 420 C. Each period contained a layer with AlAs quantum dots of nominal thickness of 2.4 monolayers and a 12-nm-thick layer of InAs. Sample C consisted of 20 layers with InAs quantum dots of nominal thickness of 2.5 monolayers coated by a 6-nm-thick GaAs layer.

The samples in which the matrix material was a solid solution $Al_xGa_{1-x}As$ consisted of five periods, each of which contained a 8-nm-thick layer of $Al_xGa_{1-x}As$ and a layer with InAs quantum dots. The content of aluminum was 0, 0.15, 0.25, 0.5, and 0.75. The structures were coated by a 20-nm-thick layer of GaAs.

The growth process was controlled by the reflection high-energy electron diffraction technique. According to the diffraction data, in all the samples, the transition from two-dimensional to three-dimensional growth mode (the onset of the formation of quantum dots) occurs after depositing 19 monolayers of the quantum-dot material. After the formation of quantum dots, the first 8 nm of the AlAs layer was grown at the same temperature as the quantum dots (500 C). Then, the temperature was raised to 600 C, and the remaining part of the AlAs layer was deposited.

The Raman spectra were recorded at a temperature of 80 K by a Dilor XY800 spectrometer. Ar^+- and Kr^+-lasers with wavelengths of 514.5 nm and 647.1 nm were used for the excitation. The spectra were measured in the geometry of backward scattering from a plane surface and from the butt ends of the samples oriented in the (110) plane. The following scattering geometries were used: $z(xx)\bar{z}$, $z(yx)\bar{z}$, $y'(zx')\bar{y}'$, and $y'(x'x')\bar{y}'$, where the axes x, y, z, x', and y' were parallel to the directions [100], [010], [001], $[1\bar{1}0]$, and [110], respectively. In the experiments with the geometry of backward scattering from a butt end, we used a microscope that allowed us to focus a laser beam to a spot of 1 μm in diameter. The spectral resolution was 2 cm^{-1} throughout the spectral range.

4. RESULTS AND DISCUSSION

To control the quality of the samples and to determine their structural parameters, we used high-resolution transmission electron microscopy. The cross sections of the samples shown in Fig. 3 indicate that InAs quantum dots are lens-shaped (samples A and C) and AlAs quantum dots are spheroidal (sample B). InAs quantum dots have a base of about 10 nm and a height of about 1.5 nm. According to the images obtained by an electron microscope, the average size of AlAs quantum dots is 4–5 nm at the base and 2–4 nm in height.

Figure 4 represents the Raman spectra of the structures A, B, and C measured in different scattering geometries that allow one to observe localized TO, LO, and/or interface phonons. According to the selection rules for plane superlattices, only LO phonons manifest themselves in the $z(yx)\bar{z}$ and $y'(x'x')\bar{y}'$ scattering geom-

etries and only TO phonons, in the $y'(zx')\bar{y}'$ geometry. In the $z(yx)\bar{z}$ and $z(xx)\bar{z}$ scattering geometries, interface phonons may appear in the resonance conditions. The figure shows that these selection rules also hold for the investigated structures with quantum dots.

For example, TO and LO phonons in the matrix materials of the samples A, B, and C are observed in allowed scattering geometries at the frequencies 359 and 402 cm^{-1} (AlAs), 216 and 235 cm^{-1} (InAs), and 267 and 291 cm^{-1} (GaAs), respectively. The frequencies of the observed TO and LO phonons are close to the values of frequencies in bulk materials. Note that the Raman spectra of all samples exhibit features corresponding to the TO and LO phonons in the GaAs substrate (267 and 291 cm^{-1}).

Figure 4 shows that, at frequencies of 386, 228, and 277 cm^{-1}, which lie approximately at the midpoint between the frequencies of the TO and LO phonons, the spectra exhibit features associated with the interface phonons in AlAs, InAs, and GaAs matrices, respectively. These features will be discussed below.

The frequencies of optical phonons localized in quantum dots differ from the frequencies in bulk materials. For example, in samples A and C, the frequencies of TO and LO phonons in InAs quantum dots are shifted by 10–15 cm^{-1} to higher frequencies with respect to the frequencies of bulk phonons in InAs due to mechanical stresses in quantum dots. The lattice constant of InAs (0.60583 nm) is greater than that of GaAs (0.565325 nm) and AlAs (5.66 nm); hence, mechanical stresses in InAs quantum dots in AlAs and GaAs matrices have the same sign: quantum dots experience contraction along the layers in which they are situated and expansion in the direction of growth of the structure [13].

The signs of mechanical stresses in sample B are reversed, which gives rise to a low-frequency shift (30–40 cm^{-1}) of the optical phonons localized in AlAs quantum dots of sample C [13].

Just as in the case of interface phonons in a matrix, the frequencies of interface phonons in quantum dots lie between the frequencies of TO and LO phonons localized in quantum dots. The frequency of an interface phonon in InAs quantum dots in sample A can be determined from the decomposition of the spectrum in the frequency region of optical phonons in InAs into two Lorentz curves that correspond to the lines of interface and LO phonons, as is shown in Fig. 4 by dashed lines, and is equal to 242 cm^{-1}. The line of interface phonons in AlAs quantum dots in sample B is observed at a frequency of 348 cm2–1, whereas sample C does not exhibit features corresponding to the interface phonons in InAs.

Now, let us consider a system in which the matrix material is a ternary solid solution $Al_xGa_{1-x}As$.

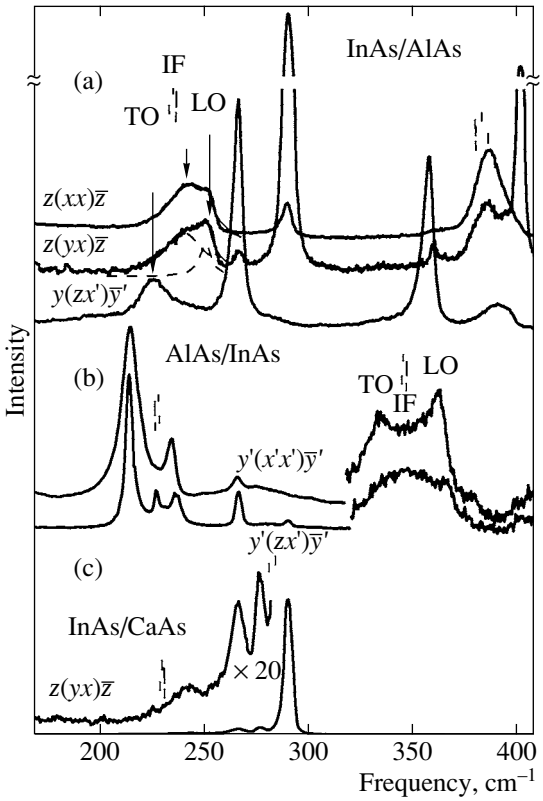

Fig. 4. Experimental Raman spectra of (a) InAs/AlAs, (b) AlAs/InAs, and (c) InAs/GaAs quantum-dot structures. Vertical bars over the graphs indicate the calculated frequencies of interface modes, and vertical arrows indicate the features corresponding to TO and LO phonons in InAs/AlAs. The excitation energy of a laser is equal to 2.41 eV (514.5 nm) (spectra (a) and (b)) and 1.91 eV (647.1 nm) (spectrum (c)).

Figure 5 represents the experimental Raman spectra of $InAs/Al_xGa_{1-x}As$ structures with InAs quantum dots for various values of x recorded in the $z(xx)\bar{z}$ and $z(xy)\bar{z}$ scattering geometries in the spectral bands of optical phonons in InAs, GaAs, and AlAs. According to the selection rules for the Raman scattering, $InAs/Al_xGa_{1-x}As$ planar structures should exhibit LO phonons in the $z(xy)\bar{z}$ scattering geometry and interface phonons in the $z(xx)\bar{z}$ scattering geometry under resonance conditions. Figure 5 shows that these selection rules are also valid for structures with quantum dots. The Raman spectra recorded in the $z(xy)\bar{z}$ geometry predominantly exhibit LO phonons of InAs quantum dots and GaAs-like and AlAs-like LO phonons of the solid solution. In the $z(xx)\bar{z}$ geometry, one can observe additional features associated with interface phonons in the frequency range between TO and LO phonons in GaAs and AlAs.

In the frequency range corresponding to optical phonons, InAs exhibits wideband features associated with the contribution of both interface and LO phonons

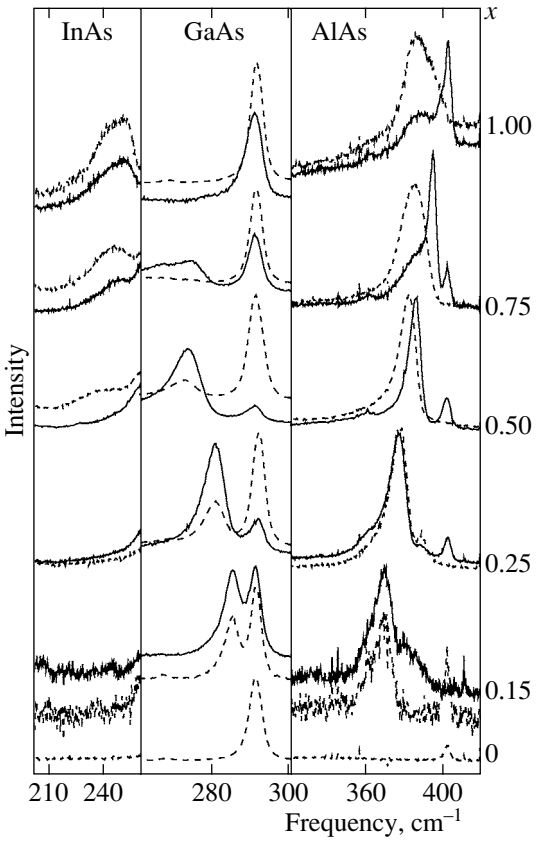

Fig. 5. Experimental Raman spectra of an InAs/$Al_xGa_{1-x}As$ structure for different values of x. Dashed lines show the spectra measured in the $z(xx)\bar{z}$ scattering geometry, and solid lines indicate the spectra measured in the $z(xy)\bar{z}$ scattering geometry. The excitation energy of a laser is equal to 1.91 eV (647.1 nm). The intensity scales of Raman scattering are different in the three parts of the spectrum.

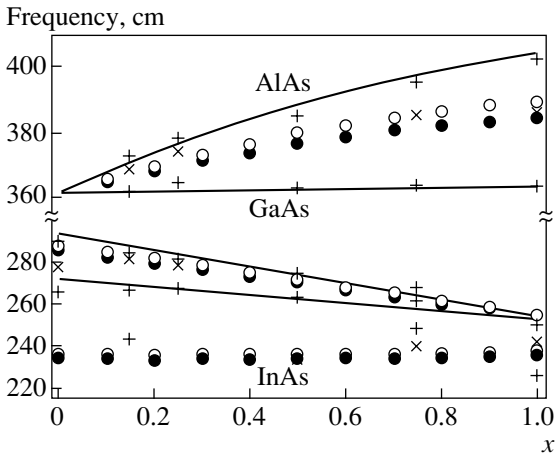

Fig. 6. Frequencies of interface phonons as a function of the composition of the $Al_xGa_{1-x}As$ matrix. The experimental values of AlAs- and GaAs-like optical (+) and interface (×) phonons are obtained from the analysis of Raman spectra. Solid lines correspond to the values of AlAs- and GaAs-like phonons in bulk AlGaAs versus the concentration of Al [14]. Calculated values of the frequencies of interface phonons in the (1, 0) and (1, 1) modes are shown by the symbols (○) and (●).

in InAs quantum dots to the Raman scattering. The frequencies of these features virtually do not depend on the composition of the solid solution of the matrix. As the concentration of aluminum increases, the intensity of Raman scattering by the phonons of InAs quantum dots decreases, which may be attributed to the decrease in the energy of interband transitions in InAs quantum dots from 1.9 eV to 1.1 eV (the excitation energy is equal to 1.91 eV). As pointed out above, the vibrational spectrum of a AlGaAs matrix has a two-mode character. As the concentration of aluminum decreases, the frequency of an AlAs-like LO phonon decreases from 403 cm^{-1} (for $x = 1$) to 386 cm^{-1} (for $x = 0.5$). In the $z(xx)\bar{z}$ geometry, this spectrum exhibits a feature that corresponds to a line of interface phonons whose frequencies decrease from 386 cm^{-1} (for $x = 1$) to 381 cm^{-1} (for $x = 0.5$). Because of the small LO–TO splitting of AlAs-like phonons in AlGaAs with small values of x, the lines of interface phonons and LO phonons in the Raman spectra are not resolved. In the range of frequencies of optical phonons in GaAs, one can observe an intense peak associated with an LO phonon in the GaAs substrate (291 cm^{-1}) and an asymmetric feature associated with the contribution of interface and GaAs-like LO phonons, whose frequency increases, as x decreases, from 273 cm^{-1} (for $x = 0.75$) to 285 cm^{-1} (for $x = 0.15$). A fitting by Lorentz curves allows one to separate the contributions of interface and LO phonons. The results of the fitting and the experimental results obtained from the Raman spectra are shown in Fig. 6.

Selection rules for the Raman scattering do not allow one to observe TO phonons in the $z(xx)\bar{z}$ and $z(yx)\bar{z}$ geometries for crystals with the symmetry of zinc blende. However, the feature at a frequency of 360 4 cm^{-1}, which weakly depends on the concentration of aluminum, is likely to correspond to an AlAs-like TO phonon and manifests itself due to the violation of the selection rules for structures with quantum dots.

The weak peak at a frequency of 402 cm^{-1} is observed in the spectra of all the samples investigated and corresponds to an LO phonon in thin spacer layers of AlAs.

Figure 6 shows that the two-mode behavior of optical phonons in the AlGaAs matrix agrees with the experimental data of [32] that were obtained for a bulk solid solution of $Al_xGa_{1-x}As$. The frequencies of interface phonons determined from the experiments are indicated by crosses.

Within the model of a dielectric continuum, we have calculated the frequencies of interface phonons in an InAs/$Al_xGa_{1-x}As$ quantum-dot structure in the approximation of spheroidal quantum dots with the parame-

ters close to the experimental values (R_p/R_e = 1/2). The form of the dielectric function of the $Al_xGa_{1-x}As$ matrix that was used in the calculation corresponds to formula (15). The circles in Fig. 6 represent the calculated InAs-, GaAs-, and AlAs-like interface modes with the quantum parameters l = 1 and m = 0, 1, because the main contribution to the Raman scattering should be made by modes with small quantum numbers [29]. One can see that the frequencies of calculated modes are in good agreement with the experimental data.

5. CONCLUSIONS

The Raman scattering of light by InAs/Al(Ga)As and AlAs/InAs periodic structures with self-organized quantum dots has been investigated. The Raman spectra measured in different scattering geometries exhibit features that correspond to optical TO and LO phonons and interface phonons. The frequencies of TO and LO phonons are displaced with respect to the corresponding values in bulk materials in view of mechanical stresses. The lines of Raman scattering by interface phonons are observed under conditions close to the resonance conditions. The frequencies of interface phonons lie in the spectral range between the frequencies of TO and LO phonons. The experimental frequencies of optical phonons have been used for calculating the frequencies of interface phonons in structures with quantum dots of different shapes in the approximation of a dielectric continuum. The frequencies of interface phonons obtained within this model depend on the shape of the quantum dots. It has been shown that the dielectric-continuum approximation is an adequate model for calculating the frequencies of interface phonons in $InAs/Al_xGa_{1-x}As$ quantum-dot structures with any value of x. In this case, it is assumed that the shape of quantum dots is close to that observed in the spectra obtained by high-resolution electron microscopy. Thus, it has been shown that the Raman spectroscopy is sensitive to the shape of quantum dots.

REFERENCES

1. D. Bimberg, M. Grundmann, F. Heinrichsdorff, *et al.*, Thin Solid Films **367**, 235 (2000).
2. D. Bimberg, M. Grundmann, and N. N. Ledentsov, *Quantum Dot Heterostructures* (Wiley, Chichester, 1999).
3. N. N. Ledentsov, V. M. Ustinov, V. A. Shchukin, *et al.*, Fiz. Tekh. Poluprovodn. (St. Petersburg) **32**, [!]385 (1998) [Semiconductors **32**, 343 (1998)].
4. J. Groenen, C. Priester, and R. Carles, Phys. Rev. B **60**, 16 013 (1999).
5. H. K. Shin, D. J. Lockwood, C. Lacelle, and P. J. Poole, J. Appl. Phys. **88**, 6423 (2000).
6. E. Martinez-Guerrero, C. Adelmann, F. Chabuel, *et al.*, Appl. Phys. Lett. **77**, 809 (2000).
7. J. Chiquito, Yu. A. Pusep, S. Mergulhao, *et al.*, Braz. J. Phys. **32**, 287 (2002).
8. Q. Xie, A. Madhukar, P. Chen, and N. Kobayashi, Phys. Rev. Lett. **75**, 2542 (1995).
9. Z. R. Wasilewski, S. Fafard, and J. P. McCarey, J. Cryst. Growth **201/202**, 1131 (1999).
10. D. A. Tenne, V. A. Haisler, A. K. Bakarov, *et al.*, Phys. Status Solidi B **224**, 25 (2001).
11. A. Milekhin, D. A. Tenne, and D. R. T. Zahn, in *Quantum Dots and Nanowires*, Ed. by Supriyo Bandyopadhyay and Hari Singh Nalwa (Am. Sci., California, 2003), p. 375.
12. A. G. Milekhin, A. I. Nikiforov, O. P. Pchelyakov, *et al.*, Pis'ma Zh. Éksp. Teor. Fiz. **81**, 33 (2005) [JETP Lett. **81**, 30 (2005)].
13. D. A. Tenne, V. A. Haisler, A. I. Toropov, *et al.*, Phys. Rev. B **61**, 13 785 (2000).
14. Z. C. Feng, A. A. Allerman, P. A. Barnes, and S. Perkowitz, Appl. Phys. Lett. **60**, 1848 (1992).
15. M. I. Vasilevskiy, Phys. Rev. B **66**, 195 326 (2002).
16. A. G. Milekhin, D. A. Tenne, A. I. Toropov, *et al.*, Phys. Status Solidi C **1**, 2629 (2004).
17. J. Groenen, A. Mlayah, R. Carles, *et al.*, Appl. Phys. Lett. **69**, 943 (1996).
18. A. G. Milekhin, A. I. Toropov, A. K. Bakarov, *et al.*, Phys. Rev. B **70**, 085 314 (2004).
19. S.-Fen. Ren, Z.-Q. Gua, and D. Lub, Solid State Commun. **113**, 273 (2000).
20. Huaxiang Fu, V. Ozolins, and Alex Zunger, Phys. Rev. B **59**, 2881 (1999).
21. G. Zanelatto, Yu. A. Pusep, N. T. Moshegov, *et al.*, J. Appl. Phys. **86**, 4387 (1999).
22. M. P. Chamberlain, C. Trallero-Giner, and M. Cardona, Phys. Rev. B **51**, 1680 (1995).
23. E. Menendez, C. Trallero-Giner, and M. Cardona, Phys. Status Solidi B **199**, 81 (1997).
24. N. Liu, H. K. Lyeo, C. K. Shih, *et al.*, Appl. Phys. Lett. **80**, 4345 (2002).
25. J. Marquez, L. Geelhaar, and K. Jacobi, Appl. Phys. Lett. **78**, 2309 (2001).
26. D. M. Bruls, J. W. A. M. Vugs, P. M. Koenraad, *et al.*, Appl. Phys. Lett. **81**, 1708 (2002).
27. A. I. Yakimov, A. V. Dvurechenskii, A. I. Nikiforov, *et al.*, Phys. Rev. B **67**, 125 318 (2003).
28. A. G. Milekhin, A. I. Toropov, A. K. Bakarov, *et al.*, Physica E (Amsterdam) **21**, 241 (2004).
29. P. A. Knipp and T. L. Reinecke, Phys. Rev. B **46**, 10 310 (1992).
30. F. Comas, C. Trallero-Giner, N. Studart, and G. E. Marques, J. Phys.: Condens. Matter **14**, 6469 (2002).
31. M. C. Klein, F. Hache, D. Ricard, and C. Flytzanis, Phys. Rev. B **42**, 11 124 (1990).
32. Z. C. Feng, S. Perkowitz, D. K. Kinell, *et al.*, Phys. Rev. B **47**, 13 466 (1993).

Translated by I. Nikitin

SPELL: 1. atomistic, 2. eigenfrequencies, 3. prolate, 4. blende